Mechanisms of Virus Assembly

Jason D. Perlmutter and Michael F. Hagan

Martin Fisher School of Physics, Brandeis University, Waltham, Massachusetts 02454; email: hagan@brandeis.edu

Annu. Rev. Phys. Chem. 2015. 66:217–39

First published online as a Review in Advance on December 17, 2014

The *Annual Review of Physical Chemistry* is online at physchem.annualreviews.org

This article's doi: 10.1146/annurev-physchem-040214-121637

Keywords

capsid, RNA packaging, simulation, kinetics, thermodynamics, membrane

Abstract

Viruses are nanoscale entities containing a nucleic acid genome encased in a protein shell called a capsid and in some cases are surrounded by a lipid bilayer membrane. This review summarizes the physics that govern the processes by which capsids assemble within their host cells and in vitro. We describe the thermodynamics and kinetics for the assembly of protein subunits into icosahedral capsid shells and how these are modified in cases in which the capsid assembles around a nucleic acid or on a lipid bilayer. We present experimental and theoretical techniques used to characterize capsid assembly, and we highlight aspects of virus assembly that are likely to receive significant attention in the near future.

1. INTRODUCTION

The formation of a virus is a remarkable feat of natural engineering. A large number (~60–10,000) of protein subunits and other components assemble from the crowded cellular milieu to form ordered, complete, reproducible structures on biologically relevant timescales. Viruses are infectious agents responsible for a significant portion of human diseases, as well as those of other animals, plants, and bacteria. Thus, it is of biomedical interest to understand their formation process, with the aim of designing antiviral therapies that block it or, alternatively, reengineering viruses for use as targeted delivery vehicles. More generally, the assembly of basic units into structures with increased size and complexity is ubiquitous in biology and is playing increasingly important roles in nanoscience. Understanding the mechanisms by which viral components coassemble may elucidate diverse classes of assembly reactions.

Viruses vary tremendously in size and complexity, ranging from the 16-nm satellite panicum mosaic virus (1), whose 826-nucleotide genome encodes for a single protein, to the micrometer-sized pandoravirus, whose 2.5-megabase genome is larger than some bacterial genomes and encodes for 2,556 putative proteins (2). However, viruses share a common body plan, consisting of a genome, which can be single stranded (ss) or double stranded (ds) and can be RNA or DNA, surrounded by a protective container, which is usually a protein shell called a capsid. For enveloped viruses (e.g., HIV and influenza), the capsid is additionally surrounded by a lipid bilayer acquired from the host cell. The formation of an infectious virion requires the assembly of the capsid, envelopment by a membrane (if enveloped), and packaging of the nucleic acid genome within. Many viruses with single-stranded genomes assemble spontaneously around their genomes, as demonstrated in 1955 by the experiments of Fraenkel-Conrat & Williams (3) in which tobacco mosaic virus RNA and capsid proteins spontaneously assembled into infectious virions in vitro. In contrast, the stiffness and high charge density of dsDNA or dsRNA preclude spontaneous encapsidation (unless the genome is first complexed with nucleic acid–folding proteins). Therefore, many dsDNA viruses assemble an empty protein capsid (procapsid) and a molecular motor that hydrolyzes ATP to pump the DNA into the capsid.

This review focuses on the physics of virus assembly—how the interactions among proteins and other viral or nonviral components determine their assembly pathways and products. Although we focus on viruses, many aspects of these pathways and the factors that control them are generic to other biological or synthetic self-assembly reactions. We begin with a brief overview of virus structures, followed by a summary of the experimental and theoretical methods used to characterize the assembly process. Next, we describe the thermodynamics, kinetics, and underlying mechanisms associated with the assembly of proteins into empty capsids (Section 2). We then consider how this process is modified when the proteins assemble around nucleic acids (Section 3) or on lipid bilayer membranes (Section 4). We then briefly discuss how small molecules that modulate assembly mechanisms form a promising new class of antiviral agents (Section 5). In the latter three sections, we concentrate on recent results that were not covered in previous reviews on capsid assembly (4, 5). Finally, we conclude by discussing open questions and possible future avenues of research.

1.1. Capsid Architectures

The viral genome length, and hence the number of unique proteins that it can encode, is constrained by the requirement that it be enclosed by its capsid. Most capsids therefore comprise one or a few protein sequences arranged with a high degree of symmetry. The majority of viruses can be classified as rodlike or spherical, with the capsid proteins of rodlike viruses arranged with helical symmetry around the nucleic acid, and the capsids of most spherical viruses arranged with

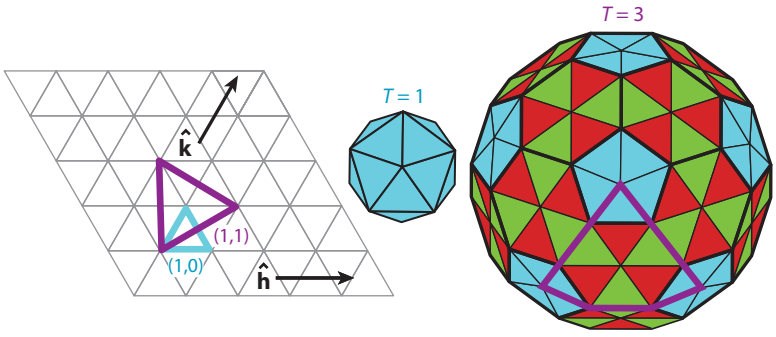

Figure 1

The geometry of icosahedral lattices. Moving h and k steps along each of the $\hat{\mathbf{h}}$ and $\hat{\mathbf{k}}$ lattice vectors results in a triangle with a triangulation number defined as $T = h^2 + hk + k^2$. The blue and purple triangles correspond to $T = 1$ and $T = 3$, respectively. The icosahedrons in the center and right images are generated by 20 such triangles, with a pentagon placed at each lattice site corresponding to a triangle vertex, and a hexagon at the remaining lattice sites. The resulting triangular facets in distinct (quasi-equivalent) environments are distinguished by color. The purple triangle from the left image is inscribed on the $T = 3$ icosahedron.

icosahedral symmetry. The number of units in a helix is arbitrary, and thus a helical capsid can accommodate a nucleic acid of any length. In contrast, icosahedral capsids are constrained by the fact that at most 60 identical subunits can form a regular polyhedron. Based on the observation that many capsids contain integer multiples of 60 proteins, Caspar & Klug (6) proposed geometrical arguments that describe how multiples of 60 proteins can be arranged with icosahedral symmetry, with individual proteins interacting through the same interfaces but taking slightly different, or quasi-equivalent, conformations (reviewed in 7, 8). A complete capsid comprises $60T$ subunits, where T is the triangulation number, which is equal to the number of distinct subunit conformations (**Figure 1**). An extensive collection of capsid structures determined from X-ray crystallography and cryo-electron microscopy data can be found on the VIPER website (**http://viperdb.scripps.edu**) (9).

1.2. Experimental and Theoretical Methods to Characterize Capsid Assembly

Below we describe the different approaches used to study capsid assembly and the complementary information they provide.

1.2.1. Bulk experiments. Capsid assembly kinetics have been measured in vitro with size-exclusion chromatography (SEC), small-angle X-ray scattering (SAXS), and light scattering (e.g., 10–17, 22) (**Figure 2*a***). The size-exclusion chromatography experiments show that under optimal assembly conditions, the only species present in detectable concentrations are either complete capsids or small protein oligomers, which we refer to as the basic assembly unit. The size of the basic assembly unit is virus dependent and ranges from two to six proteins. Under certain conditions, the intensity of the light-scattering signal is proportional to the mass-averaged molecular weight of species in solution, which closely tracks the fraction of subunits in capsids (provided that intermediate concentrations remain small).

1.2.2. Single-molecule techniques. It is difficult to characterize assembly pathways with bulk techniques because most intermediates are transient. Techniques that monitor individual capsids have begun to address this limitation. For example, a Coulter counter–like apparatus that uses

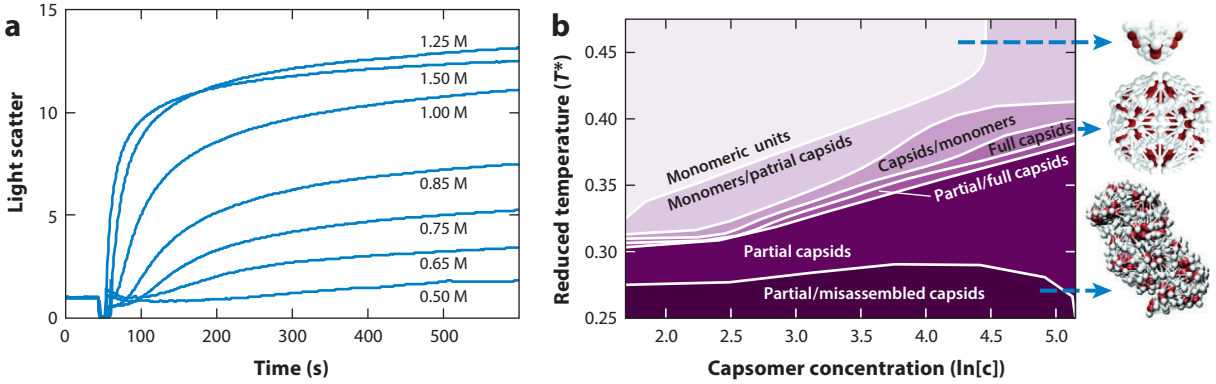

Figure 2

(*a*) Light scattering measured as a function of time for a 5-μM dimer of hepatitis B virus capsid protein at the indicated ionic strengths. Panel *a* reprinted with permission from Reference 11. Copyright 1999 American Chemical Society. (*b*) Assembly products at long times for a 20-subunit icosahedral shell as a function of temperature (i.e., inverse of the interaction strength) and particle concentration. Representative structures for several regions are shown on the right. Panel *b* adapted with permission from Reference 43. Copyright 2007 American Chemical Society.

resistive pulse sensing to identify the passage of individual capsids through nanopores was able to distinguish between $T = 3$ and $T = 4$ hepatitis B virus (HBV) capsids (18). Mass spectrometry has been used to characterize key intermediates and assembly pathways for several viruses (19–21, 23). Fluorescent labeling of capsid proteins or RNA has enabled tracking of the assembly and protein-RNA association of HIV capsids in cells (24, 25). Borodavka et al. (26) used single-molecule fluorescence correlation spectroscopy to monitor the hydrodynamic radii of assembling nucleocapsid complexes (Section 3.5).

1.2.3. Theoretical models. Zlotnick and coworkers (11, 27, 28) developed an approach to describe capsid assembly kinetics with a system of rate equations for the time evolution of concentrations of intermediates. Their equations are analogous to the classic Becker-Döring rate equations for cluster concentrations in a system undergoing crystallization (29), except that the capsids terminate at a finite size. The equations are made tractable by assuming one or a few structures for each intermediate size. Continuum-level descriptions of assembly dynamics (with further simplifications) have also been developed (30, 31). The assumption of one structure per intermediate size can be relaxed by enumerating pathways (32); in an alternative approach (33–37), pathways consistent with a master equation are stochastically sampled using the BKL (Bortz-Kalos-Lebowitz) or Gillespie algorithm (38, 39).

1.2.4. Particle-based dynamics simulations. The approaches described in the previous paragraph must pre-assume the state space (i.e., the possible structures of partial capsid intermediates). This limitation can be relaxed by performing simulations that explicitly track the dynamics of subunit positions and orientations using molecular dynamics, Brownian dynamics, or other equations of motion. Several groups have developed coarse-grained models for subunits, which have excluded-volume geometries and orientation-dependent attractions designed such that the lowest-energy structure is a shell with icosahedral symmetry (e.g., 40–51). A recent approach used particle-based simulations to systematically derive Markov state models, which can then be simulated using methods described in the previous paragraph (52).

2. EMPTY CAPSID ASSEMBLY

We begin this section by analyzing the formation process of an empty capsid. Although this process is most relevant to viruses that first form empty procapsids during assembly, it also provides a useful starting point to understand coassembly with nucleic acids, lipid membranes, or scaffolding proteins. Although we focus on icosahedral capsids, many viruses have nonicosahedral capsids, and the capsid proteins of some icosahedral viruses can form other structures, including sheets, tubes, and multilayered shells, depending on solution conditions (53).

2.1. Thermodynamics of Assembly

We consider the thermodynamics for a system of identical protein subunits that can assemble into empty $T = 1$ capsids. To simplify the presentation, we assume that there is one dominant intermediate species for each number of subunits n. Minimizing the total free energy under the constraint of a fixed total subunit concentration $c_T = \sum_{n=1}^{N} n c_n$ results in the law of mass action for the equilibrium concentration of each species c_n (5, 27, 54, 55):

$$c_n v_0 = (c_1 v_0)^n \exp(-G_n^{\text{cap}}/k_B T), \tag{1}$$

with v_0 the standard state volume and $k_B T$ the thermal energy. Here G_n^{cap} is the free energy due to subunit-subunit interactions for intermediate n. Zlotnick and colleagues (27, 28) developed a class of models in which the interaction free energy is proportional to the number of subunit-subunit contacts: $G_n^{\text{cap}} = g_b C_n - T S_n$, with C_n the number of subunit-subunit contacts in an intermediate, g_b the subunit-subunit binding free energy, and S_n accounts for degeneracy.

Under most conditions at equilibrium, almost all the subunits are found in complete capsids or as free subunits (5, 27). This prediction arises from virtually any model for the assembly of finite-size structures (e.g., capsids and micelles) in which the interaction free energy G_n^{cap} is minimum for one structure ($n = N$) and the total subunit concentration is conserved (54). Under these conditions, Equation 1 can be simplified by neglecting all intermediates except free subunits or complete capsids so that $c_T = c_1 + N c_N$, with N the number of subunits in a complete capsid (i.e., a two-state approximation). Then, in the limit $N \gg 1$, the fraction of subunits in capsids, $f_c = N c_N / c_T$, is given by

$$\begin{aligned} f_c &\approx \left(\frac{c_T}{c^*}\right)^N \ll 1 \quad \text{for } c_T \ll c^*, \\ &\approx 1 - \frac{c^*}{c_T} \qquad \text{for } c_T \gg c^*, \end{aligned} \tag{2}$$

with the pseudo-critical subunit concentration $c^* \approx v_0^{-1} \exp(G_N^{\text{cap}}/N k_B T)$ below which there is no assembly (5, 30).

Zlotnick and coworkers (56) have shown that the assembly of HBV can be captured by Equation 2 using the subunit-subunit binding free energy g_b as a fit parameter. Their data show that productive assembly requires weak binding free energies, on the order of $g_b = 4$ kcal/mol ($6.7 k_B T$), using a standard state reference concentration of 1 M. The requirement for weak interactions appears to be quite general, for reasons discussed in Section 2.4 (see also 57 in this volume).

2.2. Assembly Driving Forces

Equation 1 reflects the fact that the formation of an ordered capsid reduces the translational entropy of its constituent subunits and thus must be driven by favorable interactions that overcome this penalty. These interactions (and changes in subunit rotational entropy) are described by the factor G^{cap}. In many cases, assembly is primarily driven by hydrophobic interactions, attenuated by electrostatics (58, 59) with directional specificity imposed by electrostatic, van der Waals, and

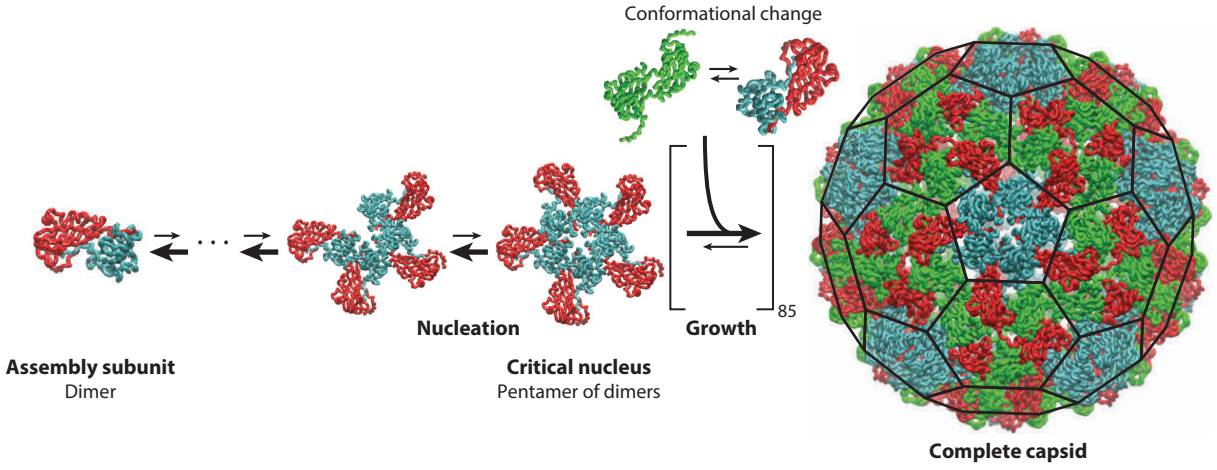

Figure 3

Schematic illustration of the assembly mechanism for cowpea chlorotic mottle virus (CCMV) (12). In the nucleation phase, the addition of capsid protein dimers is unfavorable until the critical nucleus is reached. Subsequent additions (the growth phase) are relatively favorable, although still reversible, until the capsid is completed. Subunits must interconvert between different quasi-equivalent conformations to assemble the $T = 3$ icosahedral geometry (**Figure 1**); different conformations are distinguished by color. The diameter of the complete CCMV capsid is 28 nm.

hydrogen-bonding interactions. These interactions are short ranged under assembly conditions, with scales ranging from a few angstroms (van der Waals and hydrogen-bonding interactions) to 0.5–1 nm (hydrophobic interactions) (60). Similarly, electrostatic interactions are screened on the scale of the Debye length λ_D, which is approximately 1 nm at physiological ionic strength (150 mM) and decreases with ionic strength I according to $\lambda_D \approx 0.3/I^{1/2}$, with λ_D in nanometers and I in molar units.

2.3. Empty Capsid Assembly Mechanism

As first suggested by Prevelige and coworkers (10), empty capsids assemble by a nucleation-and-growth mechanism, in which a critical nucleus forms, followed by a growth phase in which one or a few subunits add sequentially until the capsid is completed (**Figure 3**). The critical nucleus is defined as the smallest intermediate that has a greater than 50% probability of growing to a complete capsid before disassembling. Smaller intermediates are transient, and thus formation of the critical nucleus is a rare event, with a timescale $\tau_{nuc} \sim c_1^{-n_{nuc}}$ with n_{nuc} the nucleus size (28, 61). In contrast, intermediates in the growth phase are relatively stable; thus, successive additions of subunits or small oligomers are independent, and the timescale for a capsid to complete the growth phase has a low-order dependence on the free subunit concentration (5, 61).

Owing to the geometry of an icosahedral shell, the first few intermediates have relatively few subunit-subunit contacts and are thus relatively unstable. The critical nucleus often corresponds to a small polygon (**Figure 3**) whose geometry maximizes the number of interactions; furthermore, subunit conformation changes may provide additional stabilization upon polygon formation. (In general, there can be an ensemble of critical nuclei, whose members depend on solution conditions and protein subunit concentration.) As the subunit-subunit binding free energy or the free subunit concentration decreases, small intermediates become less stable, and the critical nucleus size

increases (62). Therefore, as the subunit supersaturation decreases over the course of an assembly reaction, the critical nucleus size increases, asymptotically approaching a half capsid (5).

Similar considerations apply to capsid disassembly. The first few subunits to disassemble must break many contacts, leading to a large activation barrier. There is therefore a pronounced hysteresis between assembly and disassembly at a given set of conditions (41, 63). This condition allows capsids to be highly metastable even at infinite dilution (64), which is an important feature given that they must eventually leave their host cell to infect another. Some capsids undergo postassembly maturation processes, which further increase their stability.

2.4. Empty Capsid Assembly Kinetics and Products

Capsid assembly kinetics, whether measured by experiments (10–17) or calculated from theoretical or computational models (11, 14, 16, 27, 28, 37, 61), are sigmoidal (**Figure 2*a***). There is an initial lag phase during which capsid intermediates form, followed by rapid capsid production, and then an asymptotic approach to equilibrium during which assembly slows as nucleation barriers rise owing to the depletion of free subunits. Increasing the subunit concentration c_T or the strength of intersubunit interactions g_b (typically by decreasing pH or increasing salt concentration) initially leads to more rapid assembly. However, although thermodynamics (Equation 2) indicates that the yield of well-formed capsids monotonically increases with g_b and c_T, the yield at long but finite times is nonmonotonic with variation of these parameters (see the highest ionic strength in **Figure 2*a***) owing to kinetic traps.

These modeling and experimental studies show that there is a trade-off between interaction specificity and kinetic accessibility—more specific interactions increase the selectivity of assembly for the target structure but decrease assembly rates owing to decreased kinetic cross sections (57, 65). The outcome of this competition between thermodynamics and kinetics has been summarized by mapping kinetic phase diagrams (**Figure 2*b***), which describe the predominant assembly outcome at long but finite times as a function of the subunit concentration, interaction strength, and degree of interaction specificity. For a given interaction specificity, the kinetic phase diagram can be classified into five regimes: (*a*) no assembly at equilibrium, (*b*) prohibitive nucleation barriers, (*c*) productive assembly, (*d*) free subunit starvation kinetic traps, and (*e*) malformed capsids.

For weak interactions or low subunit concentrations, such that $c_T < c^*$ (Equation 2), assembly is unfavorable at equilibrium [regime (*a*)]. As interactions or subunit concentrations increase to $c_T \gtrsim c^*$, assembly is favorable, but does not occur on experimentally relevant timescales because of large nucleation barriers [regime (*b*)]. Further increasing interactions or subunit concentrations leads to moderate nucleation barriers and large yields of well-formed capsids on relevant timescales (which can range from seconds to hours for empty capsids) [regime (*c*)]. Finally, stronger-than-optimal interactions lead to suppressed yields owing to two forms of kinetic traps. When nucleation is fast compared to growth, too many capsids nucleate at early times, and free subunits or small intermediates are depleted before a significant number of capsids finish assembling [regime (*d*)] (11, 12, 28, 41, 43, 48). This condition occurs when the timescale required for capsids to complete the growth phase exceeds the typical nucleation timescale (5, 61).

Under sufficiently strong interactions, subunits with imperfect orientations are trapped into growing clusters by subsequent subunit additions, leading to either defective closed shells that lack icosahedral symmetry or open, spiral structures in simulations (40–43, 45) and experiments (66–68) [regime (*e*)]. The presence of these two forms of kinetic traps [regimes (*d*) and (*e*)] explains the experimental (56, 69) and computational (41, 48) observation that weak interactions are required for productive capsid assembly. These kinetic traps lead to similar constraints on interactions in other forms of assembly, such as crystallization (57).

3. CAPSID ASSEMBLY AROUND NUCLEIC ACIDS AND OTHER POLYELECTROLYTES

This section focuses on viruses for which the capsid assembles spontaneously around the viral genome during infection. This category includes most ssRNA viruses and the Hepadnaviridae (e.g., HBV), which assemble around ssRNA pregenomes that then undergo reverse transcription to yield dsDNA within the virions.

Electrostatic interactions between positive charges on capsid proteins and negative charges on RNA provide an important thermodynamic driving force for this process. For example, the capsid proteins of many negative-stranded RNA viruses bind RNA via a positively charged cleft (70). For many positive-stranded RNA viruses, the capsid proteins bind RNA via flexible terminal domains rich in basic amino acids, called arginine-rich motifs (ARMs) (71). Specific RNA sequences or chemistry is not essential for assembly, as demonstrated by early in vitro experiments in which ssRNA capsid proteins assembled around heterologous nucleic acids and even polyvinylsulfate (72, 73) and more recent experiments in which capsid proteins assembled around various negatively charged substrates (e.g., 72–85). We begin this section by describing what these experiments and theoretical models have revealed about how assembly depends on the physical characteristics of RNA or other polyelectrolytes, such as charge, size, and structure. Because of space limitations, we do not discuss studies on assembly around nonpolymeric cores (see 5, 86). We then consider mechanisms by which virus-specific interactions can enhance coassembly and enable selective packaging of the viral genome.

3.1. Thermodynamics of Assembly Around a Cargo

We consider a solution of capsid protein subunits and cores (e.g., RNA molecules) with respective total concentrations of c_T and x_T. We define a stoichiometric ratio as the ratio of available cores to the maximum number of capsids that can be assembled, $r = N x_T / c_T$. Extending Equation 1 to include interior cores results in two laws of mass action (5, 87, 88):

$$c_n v_0 = (c_1 v_0)^n \exp[-G_n^{\text{cap}}/k_B T], \tag{3}$$

$$x_n v_0 = x_0 v_0 (c_1 v_0)^n \exp[-G_n^{\text{core}}/k_B T], \tag{4}$$

with v_0 the standard state volume, c_n the concentration of species containing n subunits, x_n the concentration of cores containing n subunits, c_1 the individual subunits, and x_0 the cores with zero subunits. Equations 3 and 4 describe the assembly of empty and core-containing capsids with respective interaction free energies G^{cap} and G^{core}. As in Equation 1, G_n^{cap} is the free energy due to subunit-subunit interactions for intermediate n. The core interaction energy G^{core} includes (e.g., in the case of an RNA core) attractive protein-RNA interactions, intramolecular electrostatic repulsions, and base-pairing interactions, as well as subunit-subunit interactions. Equation 4 identifies a new critical subunit concentration, which for excess capsid protein is given by $c^{**} = \exp[G_N^{\text{core}}/N k_B T]/v_0$ (87). If the net contribution of the core to assembly is favorable ($G_N^{\text{core}} < G_N^{\text{cap}}$), core-assisted assembly can occur at concentrations below the threshold concentration for empty capsid assembly ($c^{**} < c^*$). This capability is exploited by many ssRNA viruses, whose capsids assemble only in the presence of RNA or other polyanions at physiological conditions, thus ensuring that the genome is packaged during assembly. Conversely, unfavorable core contributions, such as those that arise from the stiffness and electrostatic repulsions of dsDNA molecules, can direct assembly away from the capsid structure to other morphologies (89).

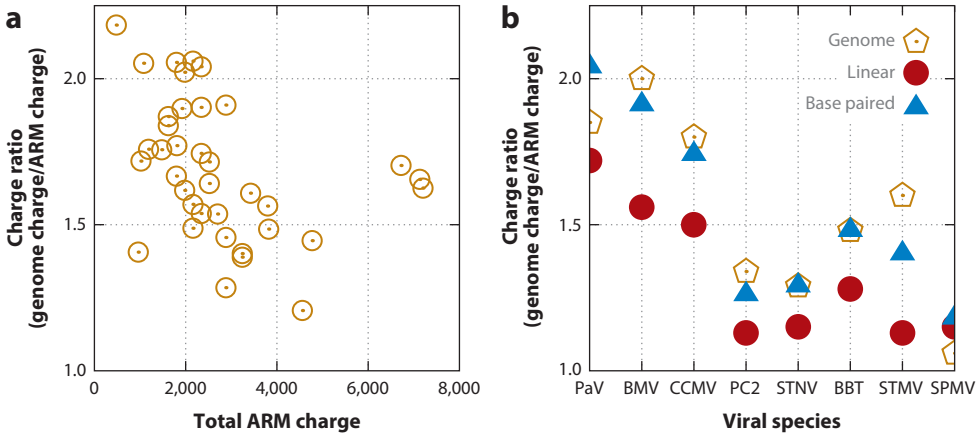

Figure 4

Relationship between genome length and capsid charge (90, 91). (*a*) The charge ratio, or number of nucleotides in the genome divided by the total positive charge on the inner capsid surface, for single-stranded RNA viruses. (*b*) The thermodynamic optimum charge ratio predicted from simulations (99) (*triangles*) compared to actual charge ratios (*pentagons*) for several viruses. Predicted optimal charge ratios in the absence of base pairing are also shown (*circles*). The thermodynamic optimum charge ratio is defined as the nucleic acid length that minimizes the free energy for encapsidating the genome divided by the positive capsid charge. Panel *b* reproduced from Reference 99. Abbreviation: ARM, arginine-rich motif.

3.2. Optimal Genome Length

It has been proposed that viral genomes face selective pressure to maintain a length that maximizes the stability of the nucleocapsid complex (i.e., minimizes G_N^{core}). In support of the importance of nonspecific electrostatics in driving RNA encapsidation, the total positive charge on the capsid inner surface correlates to the length of the genomic RNA for a diverse group of ssRNA viruses (90, 91) (**Figure 4**). Furthermore, changing the capsid charge alters the amount of cargo encapsidated in cells and in vitro (92–96), although the effect of mutations on the amounts and sequences of packaged RNA can depend on factors other than charge (95, 97). Importantly, ssRNA viruses are consistently overcharged, with typical charge ratios of $r_{\text{charge}} = |\text{NA charge}|/|\text{protein charge}|$ in the range $1.5 \leq r_{\text{charge}} \leq 2$ (**Figure 4**). In vitro competition assays in which different species of RNAs competed for packaging demonstrated that longer RNAs (up to the viral genome length) are preferentially packaged over shorter RNAs (98), indicating that overcharged genomes are optimal for packaging even in the absence of cell-specific factors.

Overcharged: in this context, indicates that the negative charge on the cargo exceeds the total positive charge on the inner surface of capsid proteins; note that the structure is still charge neutral because of the presence of counterions

3.2.1. Optimal length for encapsulation of a linear polyelectrolyte. Motivated by these observations, researchers theoretically and computationally calculated how the free energy $F_{\text{encap}}(L)$ to encapsulate a linear polyelectrolyte varies with its length L (reviewed in 5, 86). Several works performed self-consistent field theory calculations in which $F(L)$ is calculated from a continuum description of polymer conformational statistics coupled to the Poisson-Boltzmann equation. Whereas van der Schoot & Bruinsma (100) predicted an optimal charge ratio of $r_{\text{charge}} = 2$, most subsequent calculations predicted $r_{\text{charge}} \lesssim 1$ (86, 90, 95, 101, 102). Belyi & Muthukumar (90) noted that if the charge on the RNA and the peptide tails were renormalized according to counterion condensation theory (103), overcharging would be predicted; however, the condensed counterions are released by RNA-peptide association, and thus the charge cannot simply be renormalized (99). Ting et al. (102) found that the optimal charge ratio varies with capsid volume and

the charge density on capsid protein ARMs (i.e., there is no single optimal charge ratio). Because the model predicted $r_{charge} < 1$ in all cases, they suggested that a Donnan potential arising from negatively charged macromolecules within cells drives overcharging. However, the subsequent in vitro competition assays (98) demonstrated that overcharging is optimal for assembly in the absence of a Donnan potential.

Perlmutter et al. (99) used a coarse-grained particle-based computational model, in which ARMs were represented as flexible polyelectrolytes affixed to capsid subunits, to determine the optimal lengths of encapsulated polyelectrolytes and nucleic acids as functions of capsid size, ARM charge, and ionic strength. The model predicted overcharging ($r_{charge} > 1$) in all cases. Optimal lengths predicted by the model for several specific viruses closely matched genome lengths for those viruses (**Figure 4*b***). Overcharging was found to arise because only a fraction of encapsulated polymer segments can closely interact with positive capsid charges (i.e., within a Debye length). Consequently, packaging of multiple short polyelectrolytes will lead to reduced or no overcharging. The thermodynamic optimal lengths closely matched the lengths that optimized the yield of long but finite-time dynamical simulations, indicating a connection between the thermostability and optimal assembly of a viral particle.

3.2.2. Effect of RNA base pairing. Approximately 50–60% of nucleotides undergo intramolecular base pairing in ssRNA molecules, leading to compact, branched structures, as recently visualized using cryo-electron microscopy (104). Although a self-consistent field theory predicted no difference between the optimal lengths for linear polyelectrolytes and compact star architectures (102), subsequent theory (105) and simulations (99) found that branching consistent with the structures of base-paired RNA increases the optimal genome length as compared to a linear polyelectrolyte, by compensating for intramolecular charge repulsions and by favoring compact conformations (**Figure 4*b***). Based on secondary structure predictions, Yoffe et al. (106) suggested that viral RNA tends to have a more compact tertiary structure than cellular RNA with equal numbers of nucleotides, which could favor assembly around the viral RNA.

3.3. Assembly at Nonoptimal Parameters

The previous section showed that, for a given capsid protein and solution conditions, there is a length of RNA for which assembly is optimal. To understand the effect of perturbing parameters from these optimal values, researchers characterized in vitro assembly products by electron microscopy (e.g., 76, 78, 98, 108, 109) or SAXS (16, 17) as functions of subunit and RNA concentrations, subunit-subunit interactions (controlled by pH, ionic strength, and protein sequence), and subunit-cargo interactions (controlled by ionic strength and protein-RNA binding domains). In addition, several groups performed Brownian dynamics simulations in which coarse-grained triangular or pentameric subunits assemble around flexible polyelectrolytes (49, 50, 99, 110–112), semiflexible polyelectrolytes (112), or model nucleic acids (99). In both experiments and simulations, parameters must be carefully tuned to achieve high yields of well-formed capsids. **Figure 5** shows an example simulation phase diagram illustrating some of the alternative products that form at nonoptimal parameters.

Assembly around polymers with nonoptimal lengths leads to several outcomes. The first is polymorphism, or the formation of capsids with different triangulation numbers, T (**Figure 1**). Cowpea chlorotic mottle virus (CCMV) capsid proteins (which form native $T = 3$ capsids) formed $T = 3$ capsids around genomic-length RNA and pseudo–$T = 2$ capsids around shorter RNAs (98, 108). The favored polymorph depends on RNA length, the preferred curvature of capsid protein-protein interactions (i.e., spontaneous curvature; Section 4.1), and stoichiometry (76, 87). For

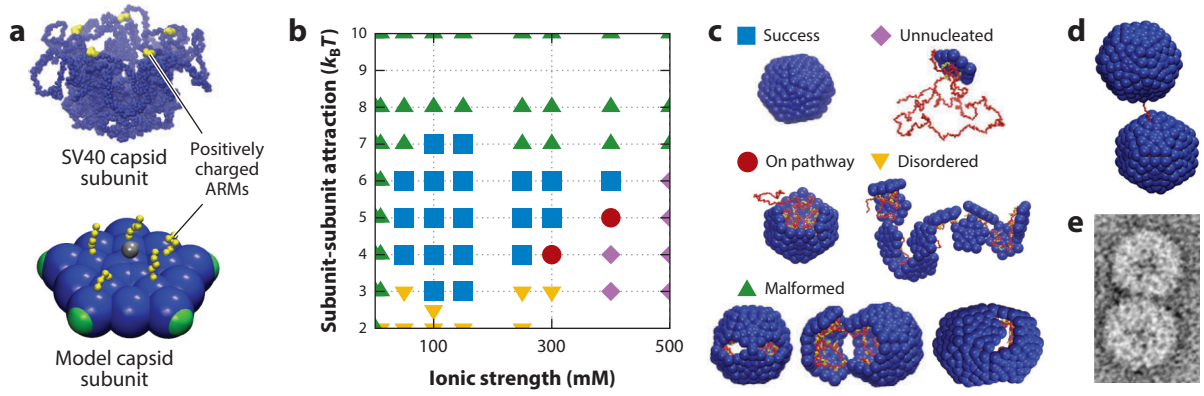

Figure 5

(*a*) Crystal structure of the SV40 basic assembly unit (107), which is a homopentamer of the capsid protein, and a coarse-grained model pentameric subunit. The locations of the positively charged arginine-rich motifs (ARMs) are shown in yellow (most of the ARM residues are not resolved in the crystal structure). (*b*) The dominant products of assembly around a linear polyelectrolyte as a function of ionic strength and subunit-subunit interaction strength at thermodynamically optimal polyelectrolyte lengths, which vary from 350 to 575 depending on the ionic strength. (*c*) Simulation snapshots exemplifying the dominant assembly outcomes. (*d*) A doublet formed in simulations around a polyelectrolyte with 1,150 segments (twice the optimal length). (*e*) A doublet assembled from cowpea chlorotic mottle virus (CCMV) capsid proteins around RNA with 6,400 nucleotides (about twice the number of nucleotides encapsidated in native CCMV virions) (108). Panels *a–c* adapted from Reference 110, copyright 2014, with permission from Elsevier. Panel *e* provided by R. Garmann, C. Knobler, and W. Gelbart.

RNA significantly below the optimal length, multiple RNAs were packaged in each capsid (108, 113), as seen in coarse-grained dynamics simulations with short linear polyelectrolytes (111). In the experiments, capsid formation required equilibrium between multiple disordered protein-RNA complexes, leading to highly cooperative assembly (113).

Although longer-than-optimal polymers sometimes led to $T = 4$ capsids, the more common outcome was the assembly of multiplets, or multiple distinct capsids assembled around one RNA (108) or conjugated polyelectrolyte (78). RNAs that were two, three, or four times the genome length led to predominantly doublets (**Figure 5*d*,*e***), triplets, and quadruplets, respectively. An early study likely also observed doublets, although the structures could not be confirmed (72), and doublet dodedecadron capsids were recently observed for the assembly of SV40 capsid proteins around certain lengths of RNA (17). Simulations independently predicted the formation of doublets around polyelectrolytes with about twice the optimal length (49, 99, 114) (**Figure 5*d***). At lengths only slightly greater than optimal, simulations predicted malformed but single capsids (49, 50, 99). However, these malformations may be difficult to resolve experimentally.

3.4. Assembly Mechanisms

Simulations (49, 110) showed that two classes of assembly mechanisms occur around RNA or a linear polymer (**Figure 6**). One closely resembles the nucleation-and-growth mechanism found for empty capsid assembly, except that the polymer stabilizes protein-protein interactions and can enhance the flux of proteins to the assembling capsid (115). A small partial capsid first nucleates on the polymer, followed by a growth phase in which one or a few subunits sequentially and reversibly add to the partial capsid. In the alternative mechanism, first proposed by McPherson (116) and then others (49, 117, 118), subunits adsorb onto the polymer en masse in a disordered fashion and then cooperatively rearrange to form an ordered capsid. Simulations predicted that the assembly

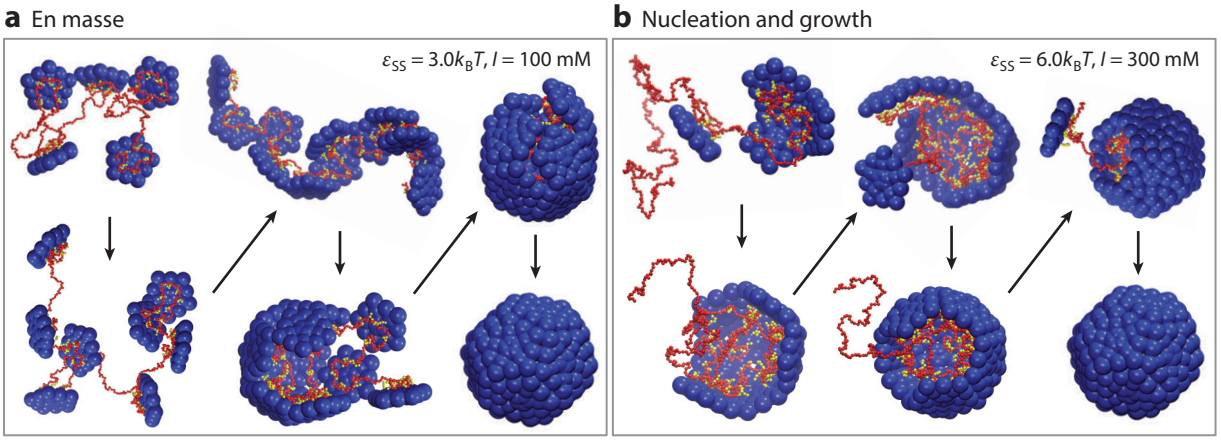

Figure 6

Two mechanisms for assembly around a polyelectrolyte (110). (*a*) Low ionic strength (strong subunit-polyelectrolyte interactions) and weak subunit-subunit interactions lead to the en masse mechanism typified by disordered intermediates. (*b*) High ionic strength (weak subunit-polymer interactions) and strong subunit-subunit interactions lead to the nucleation-and-growth mechanism in which an ordered nucleus forms on the polymer followed by the sequential addition of subunits. Figure reprinted from Reference 110, copyright 2014, with permission from Elsevier.

mechanism can be tuned by solution conditions and capsid protein-protein interactions (110). The nucleation-and-growth mechanism is favored by weak protein-polymer association (high salt concentration) and strong protein-protein interactions [typically low pH (89)], whereas the en masse mechanism arises for lower salt concentrations and weaker protein-protein interactions.

Observations in vitro suggest that both mechanisms are viable. Time-resolved SAXS experiments monitoring SV40 capsid proteins assembling around ssRNA produced scattering profiles that could be decomposed into profiles corresponding to unassembled components (RNA + protein subunits) and complete capsids (16). The absence of detectable intermediates suggested that assembly follows the nucleation-and-growth mechanism. In support of this conclusion, simulations (110) showed that the disordered intermediates arising in en masse pathways led to measurably different SAXS profiles, whereas profiles from nucleation-and-growth trajectories are consistent with the experimental observations. Other observations suggest that virus-like particles can assemble through the en masse mechanism. Researchers found that in vitro CCMV assembly was most productive when performed in two steps (108, 109, 119). First, at low salt concentrations (strong protein-RNA interactions) and neutral pH (weak protein-protein interactions), the proteins undergo extensive but disordered adsorption onto RNA. Subsequently, pH is reduced to enhance protein-protein binding, leading to the formation of ordered capsids (109). Similarly, capsid protein assembly around charge-functionalized nanoparticles was recently observed to initially proceed through nonspecific aggregation of proteins and nanoparticles, followed by the gradual extrusion of complete capsids formed around nanoparticles (84).

The CCMV experiments (108, 109, 119) found that complete encapsidation of all RNA present in solution requires a significant excess of capsid protein, such that the positive charges in protein ARMs balance the negative RNA charge. [As mentioned above, in the complete capsid, the negative RNA charge significantly exceeds the positive ARM charge (Section 3.2)]. This criterion was attributed to the fact that the disordered protein-RNA complexes that form during the first step of assembly are charge balanced. During capsid formation (the second step), excess proteins are

displaced to the exterior, where their positive ARM charges interact with negative residues on the outer surface of the capsid (119).

3.5. Sequence-Specific Contributions to Assembly and Selective Genome Packaging

To be infectious, a virion must assemble specifically around the viral genome amid a panoply of cellular RNA molecules. Many viruses achieve high specificity; for example, a recent quantitative analysis found that flock house virus particles are 99% selective for the viral RNA (120). Structure- and sequence-specific RNA-protein interactions may be a widespread mechanism of achieving specificity by promoting assembly around the viral genome [although not all viruses are selective for their genomic RNA in vitro (96, 98), suggesting the importance of cell-specific factors].

Several studies suggest that the specific folded structure of the genomic RNA may enhance assembly. Based on the crystal structure of satellite tobacco mosaic virus (STMV), which shows 30 double-stranded helical segments interacting with the capsid inner surface (121, 122), McPherson and coworkers (123) proposed that, during assembly, the STMV genome forms a conformation comprising linearly connected stem loops, which sequentially bind capsid proteins. Using the crystal structure as constraints, Schroeder et al. (124) combined chemical probing and computational methods to predict an RNA secondary structure containing 30 stem loops. Simulation of the complete STMV capsid with atomic resolution demonstrated that this secondary structure is consistent with the crystal structure (125). More recently, two studies (126, 127) used the chemical probe method SHAPE to characterize unencapsidated STMV RNA. These analyses were not restricted to stem loops and found secondary structures that differed significantly from the encapsidated, stem-loop structure. Interestingly, the primary probing data are similar for the encapsidated and unencapsidated RNA, suggesting that many of the same nucleic acids are base paired in both cases (126).

Extensive evidence shows that packaging signals, or short RNA sequences that are specifically bound by capsid proteins, play significant roles in controlling assembly pathways for some viruses (reviewed in 128, 129). Packaging signals have been identified for several viruses, including HIV (130–132), MS2, and satellite tobacco necrosis virus (133–135), and a number of plant viruses (128). Combining identified packaging signals with geometric constraints derived from electron density maps of MS2 capsids led to a structure of the encapsidated genome (134). Earlier work using mass spectrometry (19), coarse-grained simulations (136), and kinetic models (137) suggested that RNA binding drives a conformational switch in the MS2 capsid protein and identified two dominant pathways for MS2 assembly. Using Gillespie algorithm simulations (Section 1.2), Dykeman et al. showed that packaging signals could enhance yields of capsids assembling around RNA in comparison to a polymer cargo with uniform interactions (36) and that specificity for the genomic RNA can be enhanced by time-dependent capsid protein production rates in bacteria (138).

Borodavka et al. (26) made a striking observation supporting an active, sequence-specific role of the genome by using single-molecule fluorescence correlation spectroscopy to monitor the hydrodynamic radii R_H of nucleocapsid complexes. Assembly around genomic RNAs was characterized by either constant R_H or, in some trajectories, a collapsed complex followed by a gradual increase in size to that of an assembled capsid. In contrast, assembly around heterologous RNA led to an increase in R_H before eventually decreasing to the size of the capsid. The different assembly pathways were attributed to the presence of packaging signals in the genomic RNA. The collapsed structures are reminiscent of a previous observation (139) in which incubation of CCMV RNA with substoichiometric concentrations of capsid proteins led to a compact nucleocapsid complex that triggered rapid assembly upon the introduction of additional capsid proteins.

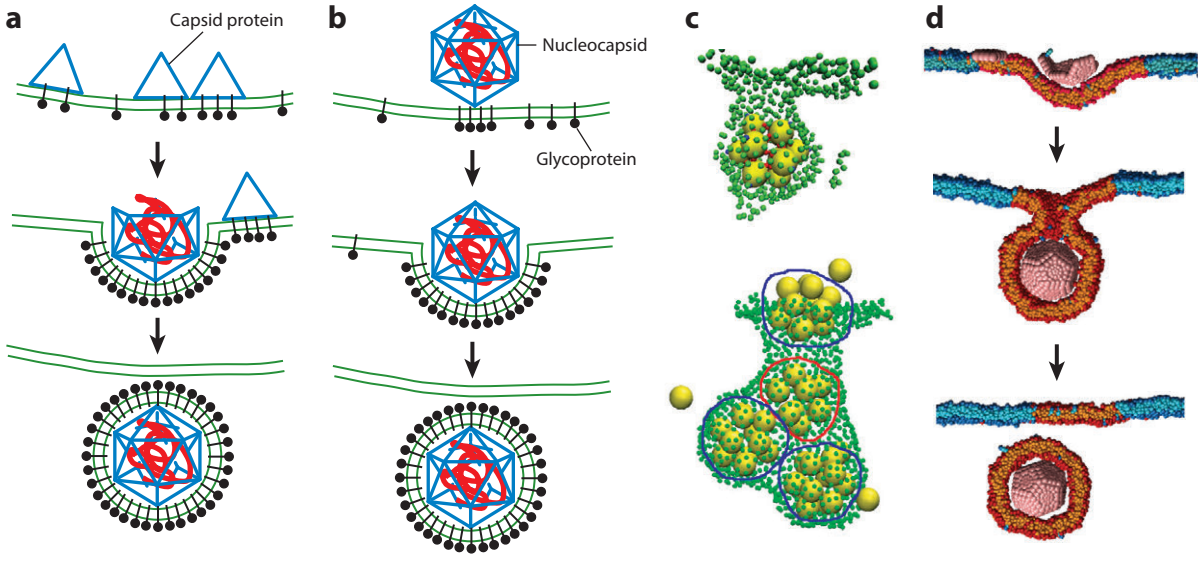

Figure 7

Viral budding pathways. (*a*,*b*) Schematic illustrations of the two classes of budding pathways for enveloped viruses. (*a*) The assembly of capsid proteins (*blue*) drives budding and the recruitment of glycoproteins (e.g., type C retroviruses). (*b*) Glycoproteins (*black*) drive budding of a preassembled nucleocapsid core (e.g., alphaviruses). (*c*) Snapshots from simulations in which patchy sphere icosahedrons assemble on and bud from a triangulated membrane. Top image in panel *c* reprinted with permission from Reference 151. Copyright 2012 by the American Physical Society. Bottom image in panel *c* reprinted from Reference 152. (*d*) Model subunits assembling on and budding from a membrane microdomain (153).

Finally, we emphasize that sequence-specific protein-RNA interactions are not the only mechanism that drives selective genome packaging in vivo; other factors include the coordination of assembly with RNA replication (128, 140). As evidence for this, in (in vitro) competition assays, HBV capsid proteins show no preference for genomic RNA over heterologous RNA with equal length (96), and CCMV capsid proteins preferentially assemble around brome mosaic virus (BMV) RNA over the genomic CCMV RNA (98). Because BMV and CCMV RNA molecules are of similar length, it was proposed that the RNA tertiary structure could drive preferential encapsidation of BMV RNA.

4. CAPSID ASSEMBLY ON MEMBRANES

In this section, we consider mechanisms by which the proteins of enveloped viruses assemble on lipid bilayers to drive budding. The passage of nanoscale particles through membranes is an extremely broad topic; we focus on viral budding driven by protein assembly.

Enveloped viruses can be divided into two groups based on how they acquire their lipid membrane envelope. For the first group, which includes influenza and type C retroviruses (e.g., HIV), the nucleocapsid core assembles on the membrane concomitant with budding (**Figure 7*a***). Capsid protein binding to membranes is driven by electrostatic interactions between positive residues on capsid proteins (e.g., the MA domain of HIV GAG) and negative charges in lipid head groups, and/or the insertion of capsid protein hydrophobic moieties (e.g., the myristoyl domain on GAG) into the bilayer (141, 142). In the second group, a core assembles in the cytoplasm prior to envelopment (reviewed in 141–143). In many families from this group, envelopment of the core is

driven by the assembly of viral transmembrane glycoproteins (GPs), which form an outer shell around the core (**Figure 7*b***), as demonstrated by the fact that GP expression alone can drive budding (144). Thus, in both groups, membrane deformation is driven at least in part by reversible protein-protein and protein-lipid interactions. However, some viruses are assisted by cellular factors that create or support membrane curvature (141, 145, 146) or cytoskeletal machinery that actively drives budding (e.g., 143, 147–149). Furthermore, the separation of budded viral particles from the host membrane (scission) is driven by cell membrane remodeling machinery (150).

Enveloped viruses have been the subject of extensive structural studies and in vivo investigations (141–143), with budding of individual capsids from cells monitored using fluorescently labeled capsid proteins and RNA (24, 25). However, there are currently no in vitro systems in which enveloped viruses assemble and bud, and information about assembly mechanisms and budding kinetics is limited in comparison to assembly in solution.

Spontaneous curvature: preferred curvature of a membrane; although the spontaneous curvature is zero for symmetric bilayers (in which the two membrane leaflets have identical compositions), asymmetric leaflet compositions or adsorption of proteins onto one side of a membrane can lead to positive or negative spontaneous curvature

4.1. Thermodynamics of Membrane-Associated Assembly

The thermodynamics of assembly on a membrane can be obtained by extending the analysis in Section 2.1 to include membrane bending energy and subunit-membrane interactions. The free energy associated with membrane deformations on scales large in comparison to the 5-nm width of a lipid bilayer can be analyzed according to the continuum elasticity (the Helfrich free energy) (54, 154):

$$E_{\text{bend}} = \int dA \left[\frac{\kappa}{2}(H - H_0)^2 + \kappa_G K \right] + \int \gamma dA, \tag{5}$$

with $H = (1/R_1 + 1/R_2)$ the mean curvature, $K = 1/(R_1 R_2)$ the Gaussian curvature, and R_1 and R_2 the principal radii of curvature at each point on the membrane neutral surface. The remaining parameters are material properties: H_0 is the membrane spontaneous curvature; κ and κ_G are the bending modulus and Gaussian modulus, respectively; and γ is the surface tension.

Because scission is actively driven by cell machinery, it is instructive to calculate the membrane bending energy for a completely budded viral particle just before scission (i.e., the bending energy of a vesicle). Because the total Gaussian curvature is constant for a fixed topology, the corresponding term in Equation 5 can be neglected (for uniform κ_G). Assuming a tensionless membrane, a roughly spherical membrane envelope, and $H_0 = 0$ (spontaneous curvature induced by protein binding is considered next), Equation 5 gives a fixed cost for any radius $E_{\text{bend}}(\text{sphere}) = 8\pi\kappa$. Lipid bilayer bending moduli are typically in the range $10 < \kappa < 30\ k_B T$, giving a membrane bending energy cost of $250–750 k_B T$ for any size virus.

This bending energy must be compensated by capsid protein–membrane, GP-GP, GP–capsid protein, and/or capsid protein–capsid protein interactions, which conspire to drive membrane curvature either through the spontaneous curvature of the protein-protein interaction geometry or directly through protein-membrane interactions. Including these effects and the bending energy equation (Equation 5) in the law of mass action (Section 2.1) predicts that assembly proceeds above a threshold subunit concentration, given by

$$\begin{aligned} c^* v_0 &\approx \exp(G_N/N k_B T), \\ G_N/N &= G_N^{\text{cap}}/N + g_{\text{sm}} + 8\pi\kappa/N, \end{aligned} \tag{6}$$

with g_{sm} accounting for the subunit-membrane interactions (per subunit) in a completely assembled and enveloped capsid. The second line of Equation 6 emphasizes that, because the membrane bending energy is independent of the capsid size, its effect is inversely proportional to the number of subunits. Thus, larger capsids are favored; perhaps relatedly, the smallest enveloped viruses

have 240 proteins ($T = 4$). If $|g_{sm}| > 8\pi\kappa/N$, assembly can proceed on the membrane for subunit concentrations at which no assembly occurs in bulk solution.

Going beyond this simple thermodynamic analysis, the statistical mechanics of budding of a preassembled nucleocapsid driven by interactions with membrane-associated GPs (**Figure 7*b***) has been considered in continuum models (155, 156). Tzlil et al. (155) identified a critical GP-capsid adhesion energy above which complete budding occurs; when complete budding occurs, they found that capsids are nearly saturated with GPs. Numerous other experimental, theoretical, and computational studies have analyzed the exit (exocytosis) or entry (endocytosis) of viruses and other nanoscale particles (reviewed in 157).

4.2. Modeling of Assembly and Budding Dynamics

The first analysis of the dynamics of assembly and budding by membrane-adsorbed capsid proteins was performed by Zhang & Nguyen (158). They developed a continuum model description, in which membrane-associated partial-capsid intermediates are represented by hemispherical shells and the membrane deformation energy is modeled by the Helfrich free energy (Equation 5). Depending on the subunit supersaturation, the model predicted complete assembly and budding or stalled partially assembled and partially wrapped states.

More recently, Matthews & Likos (151, 152) performed particle-based simulations of patchy spheres assembling into icosahedrons on a triangulated representation of a membrane (**Figure 7*c***). They found that subunit adsorption onto the membrane could drive assembly for parameters for which no assembly occurred in bulk (see Equation 6). Interestingly, the ability of the membrane to promote assembly depended nonmonotonically on the bending modulus κ, with budding suppressed by the membrane bending energy at high κ or entropic membrane fluctuations at low κ (151). Ruiz-Herrero & Hagan (153) considered an implicit solvent lipid bilayer membrane model and pentameric subunits that adsorb onto the membrane and assemble to form a dodecahedron (**Figure 7*d***). They found that, although adsorption onto the membrane promoted the formation of small partial capsids, the geometry of adsorbed subunits could introduce new barriers to assembly. Based on the observation that many enveloped viruses preferentially bud from lipid rafts (143, 159, 160), assembly was also simulated on a phase-separated membrane. Assembly and budding were significantly enhanced for certain domain sizes.

5. SMALL-MOLECULE ASSEMBLY EFFECTORS AS ANTIVIRAL AGENTS

In this section, we briefly consider small-molecule assembly effectors, which modulate assembly by perturbing capsid protein-protein interactions, altering protein conformations, or cross-linking protein–nucleic acid binding domains (for reviews, see 161, 162). These molecules have been proposed as a new class of antiviral agents that interfere with capsid assembly, genome packaging, or disassembly. This strategy has significant promise, as relatively few existing treatments target these steps of the viral life cycle.

It has been demonstrated that small molecules can stabilize the capsids of picornaviruses, inhibiting disassembly and preventing viral propagation (163, 164). Directly interfering with assembly may also be a viable strategy; for HIV, peptides and small molecules have been developed that interfere with subunit-subunit interactions and prevent assembly in vitro, as well as trigger premature disassembly and inhibit capsid maturation (161). Interestingly, two classes of small molecules have been found to interfere with HBV capsid assembly by strengthening the interaction between capsid subunits (165, 166). The heteroaryldihydropyrimidine compounds both

strengthen and subtly alter the geometry of HBV capsid protein subunit-subunit interactions, leading to malformed capsids (see Section 2.4). The phenylpropenamide compounds do not alter the capsid geometry, but by strengthening subunit-subunit interactions, they enable assembly in the absence of the genome (see Section 3.1), leading to empty capsids, which are (likely) a dead end for the HBV viral life cycle.

6. OUTLOOK

Above we present a summary of capsid assembly mechanisms, how they are influenced by nonprotein components such as nucleic acids and lipid bilayers, and some virus-specific interactions that facilitate selective genome packaging. Because most intermediates on assembly pathways remain challenging to characterize, complementary experimental and theoretical investigations will play important roles in further elucidating assembly mechanisms. As computing power and the sophistication of computational methods increase, models with increased resolution and complexity will become feasible. At the same time, new experimental capabilities to monitor the assembly of individual viruses will place additional constraints with which to more stringently test and refine these models.

For biomedical applications, it will be essential to build models that incorporate factors specific to host environments, such as molecular crowding (37), subcellular localization (167), coordinated translation and assembly (97, 138, 140), and active processes (147–149). Doing so will require more quantitative data from in vivo experiments and in vitro systems that systematically incorporate host factors, in conjunction with corresponding comprehensive models. Such combined experiments and models can reveal the features that make virus assembly so robust and identify the factors that are most sensitive to manipulation by drugs or other antiviral agents.

DISCLOSURE STATEMENT

The authors are not aware of any affiliations, memberships, funding, or financial holdings that might be perceived as affecting the objectivity of this review.

ACKNOWLEDGMENTS

This work was supported by the NIH through award R01GM108021 from the National Institute of General Medical Sciences and the NSF through award NSF-MRSEC-0820492. We thank Chuck Knobler for a critical reading of the manuscript.

LITERATURE CITED

1. Ban N, McPherson A. 1995. The structure of satellite panicum mosaic virus at 1.9 Å resolution. *Nat. Struct. Mol. Biol.* 2:882–90
2. Philippe N, Legendre M, Doutre G, Couté Y, Poirot O, et al. 2013. Pandoraviruses: amoeba viruses with genomes up to 2.5 Mb reaching that of parasitic eukaryotes. *Science* 341:281–86
3. Fraenkel-Conrat H, Williams RC. 1955. Reconstitution of active tobacco mosaic virus from its inactive protein and nucleic acid components. *Proc. Natl. Acad. Sci. USA* 41:690–98
4. Mateu MG. 2013. Assembly, stability and dynamics of virus capsids. *Arch. Biochem. Biophys.* 531:65–79
5. Hagan MF. 2014. Modeling viral capsid assembly. *Adv. Chem. Phys.* 155:1–68
6. Caspar DLD, Klug A. 1962. Physical principles in construction of regular viruses. *Cold Spring Harb. Symp. Quant. Biol.* 27:1–24

7. Johnson JE, Speir JA. 1997. Quasi-equivalent viruses: a paradigm for protein assemblies. *J. Mol. Biol.* 269:665–75
8. Zlotnick A. 2005. Theoretical aspects of virus capsid assembly. *J. Mol. Recognit.* 18:479–90
9. Reddy VS, Natarajan P, Okerberg B, Li K, Damodaran KV, et al. 2001. Virus Particle Explorer (VIPER), a website for virus capsid structures and their computational analyses. *J. Virol.* 75:11943–47
10. Prevelige PE Jr, Thomas D, King J. 1993. Nucleation and growth phases in the polymerization of coat and scaffolding subunits into icosahedral procapsid shells. *Biophys. J.* 64:824–35
11. Zlotnick A, Johnson JM, Wingfield PW, Stahl SJ, Endres D. 1999. A theoretical model successfully identifies features of hepatitis B virus capsid assembly. *Biochemistry* 38:14644–52
12. Zlotnick A, Aldrich R, Johnson JM, Ceres P, Young MJ. 2000. Mechanism of capsid assembly for an icosahedral plant virus. *Virology* 277:450–56
13. Casini GL, Graham D, Heine D, Garcea RL, Wu DT. 2004. In vitro papillomavirus capsid assembly analyzed by light scattering. *Virology* 325:320–27
14. Chen C, Kao CC, Dragnea B. 2008. Self-assembly of brome mosaic virus capsids: insights from shorter time-scale experiments. *J. Phys. Chem. A* 112:9405–12
15. Berthet-Colominas C, Cuillel M, Koch MHJ, Vachette P, Jacrot B. 1987. Kinetic study of the self-assembly of brome mosaic virus capsid. *Eur. Biophys. J.* 15:159–68
16. Kler S, Asor R, Li C, Ginsburg A, Harries D, et al. 2012. RNA encapsidation by SV40-derived nanoparticles follows a rapid two-state mechanism. *J. Am. Chem. Soc.* 134:8823–30
17. Kler S, Wang JCY, Dhason M, Oppenheim A, Zlotnick A. 2013. Scaffold properties are a key determinant of the size and shape of self-assembled virus-derived particles. *ACS Chem. Biol.* 8:2753–61
18. Zhou K, Li L, Tan Z, Zlotnick A, Jacobson SC. 2011. Characterization of hepatitis B virus capsids by resistive-pulse sensing. *J. Am. Chem. Soc.* 133:1618–21
19. Stockley PG, Rolfsson O, Thompson GS, Basnak G, Francese S, et al. 2007. A simple, RNA-mediated allosteric switch controls the pathway to formation of a $T = 3$ viral capsid. *J. Mol. Biol.* 369:541–52
20. Basnak G, Morton VL, Rolfsson O, Stonehouse NJ, Ashcroft AE, Stockley PG. 2010. Viral genomic single-stranded RNA directs the pathway toward a $T = 3$ capsid. *J. Mol. Biol.* 395:924–36
21. Uetrecht C, Barbu IM, Shoemaker GK, van Duijn E, Heck AJR. 2011. Interrogating viral capsid assembly with ion mobility-mass spectrometry. *Nat. Chem.* 3:126–32
22. Tresset G, Le Coeur C, Bryche JF, Tatou M, Zeghal M, et al. 2013. Norovirus capsid proteins self-assemble through biphasic kinetics via long-lived stave-like intermediates. *J. Am. Chem. Soc.* 135:15373–81
23. Pierson EE, Keifer DZ, Selzer L, Lee LS, Contino NC, et al. 2014. Detection of late intermediates in virus capsid assembly by charge detection mass spectrometry. *J. Am. Chem. Soc.* 136:3536–41
24. Baumgärtel V, Müller B, Lamb DC. 2012. Quantitative live-cell imaging of human immunodeficiency virus (HIV-1) assembly. *Viruses* 4:777–99
25. Jouvenet N, Simon SM, Bieniasz PD. 2011. Visualizing HIV-1 assembly. *J. Mol. Biol.* 410:501–11
26. Borodavka A, Tuma R, Stockley PG. 2012. Evidence that viral RNAs have evolved for efficient, two-stage packaging. *Proc. Natl. Acad. Sci. USA* 109:15769–74
27. Zlotnick A. 1994. To build a virus capsid: an equilibrium model of the self-assembly of polyhedral protein complexes. *J. Mol. Biol.* 241:59–67
28. Endres D, Zlotnick A. 2002. Model-based analysis of assembly kinetics for virus capsids or other spherical polymers. *Biophys. J.* 83:1217–30
29. Becker R, Döring W. 1935. Kinetische Behandlung der Keimbildung in übersättigten Dämpfen. *Ann. Phys.* 416:719–52
30. van der Schoot P, Zandi R. 2007. Kinetic theory of virus capsid assembly. *Phys. Biol.* 4:296–304
31. Morozov AY, Bruinsma RF, Rudnick J. 2009. Assembly of viruses and the pseudo-law of mass action. *J. Chem. Phys.* 131:155101
32. Moisant P, Neeman H, Zlotnick A. 2010. Exploring the paths of (virus) assembly. *Biophys. J.* 99:1350–57
33. Zhang Q, Gupta S, Emrick T, Russell T. 2006. Surface-functionalized CdSe nanorods for assembly in diblock copolymer templates. *J. Am. Chem. Soc.* 128:3898–99
34. Keef T, Micheletti C, Twarock R. 2006. Master equation approach to the assembly of viral capsids. *J. Theor. Biol.* 242:713–21

35. Hemberg M, Yaliraki S, Barahona M. 2006. Stochastic kinetics of viral capsid assembly based on detailed protein structures. *Biophys. J.* 90:3029–42
36. Dykeman EC, Stockley PG, Twarock R. 2013. Building a viral capsid in the presence of genomic RNA. *Phys. Rev. E* 87:022717
37. Smith GR, Xie L, Lee B, Schwartz R. 2014. Applying molecular crowding models to simulations of virus capsid assembly in vitro. *Biophys. J.* 106:310–20
38. Bortz AB, Kalos MH, Lebowitz JL. 1975. New algorithm for Monte Carlo simulation of Ising spin systems. *J. Comput. Phys.* 17:10–18
39. Gillespie DT. 1977. Exact stochastic simulation of coupled chemical reactions. *J. Phys. Chem.* 81:2340–61
40. Schwartz R, Shor PW, Prevelige PE Jr, Berger B. 1998. Local rules simulation of the kinetics of virus capsid self-assembly. *Biophys. J.* 75:2626–36
41. Hagan MF, Chandler D. 2006. Dynamic pathways for viral capsid assembly. *Biophys. J.* 91:42–54
42. Hicks SD, Henley CL. 2006. Irreversible growth model for virus capsid assembly. *Phys. Rev. E* 74:031912
43. Nguyen HD, Reddy VS, Brooks CL. 2007. Deciphering the kinetic mechanism of spontaneous self-assembly of icosahedral capsids. *Nano Lett.* 7:338–44
44. Wilber AW, Doye JPK, Louis AA, Noya EG, Miller MA, Wong P. 2007. Reversible self-assembly of patchy particles into monodisperse icosahedral clusters. *J. Chem. Phys.* 127:085106
45. Nguyen HD, Reddy VS, Brooks CL. 2009. Invariant polymorphism in virus capsid assembly. *J. Am. Chem. Soc.* 131:2606–14
46. Johnston IG, Louis AA, Doye JPK. 2010. Modelling the self-assembly of virus capsids. *J. Phys. Condens. Matter* 22:104101
47. Rapaport DC, Johnson JE, Skolnick J. 1999. Supramolecular self-assembly: molecular dynamics modeling of polyhedral shell formation. *Comput. Phys. Commun.* 122:231–35
48. Rapaport D. 2008. The role of reversibility in viral capsid growth: a paradigm for self-assembly. *Phys. Rev. Lett.* 101:186101
49. Elrad O, Hagan MF. 2010. Encapsulation of a polymer by an icosahedral virus. *Phys. Biol.* 7:045003
50. Mahalik JP, Muthukumar M. 2012. Langevin dynamics simulation of polymer-assisted virus-like assembly. *J. Chem. Phys.* 136:135101
51. Rapaport DC. 2012. Molecular dynamics simulation of reversibly self-assembling shells in solution using trapezoidal particles. *Phys. Rev. E* 86:051917
52. Perkett MR, Hagan MF. 2014. Using Markov state models to study self-assembly. *J. Chem. Phys.* 140:214101
53. Lavelle L, Gingery M, Phillips M, Gelbart WM, Knobler CM, et al. 2009. Phase diagram of self-assembled viral capsid protein polymorphs. *J. Phys. Chem. B* 113:3813–19
54. Safran S. 1994. *Statistical Thermodynamics of Surfaces, Interfaces, and Membranes*. New York: Addison-Wesley
55. Bruinsma RF, Gelbart WM, Reguera D, Rudnick J, Zandi R. 2003. Viral self-assembly as a thermodynamic process. *Phys. Rev. Lett.* 90:248101
56. Ceres P, Zlotnick A. 2002. Weak protein-protein interactions are sufficient to drive assembly of hepatitis B virus capsids. *Biochemistry* 41:11525–31
57. Whitelam S, Jack RL. 2015. The statistical mechanics of dynamic pathways to self-assembly. *Annu. Rev. Phys. Chem.* 66:143–63
58. del Alamo M, Mateu MG. 2005. Electrostatic repulsion, compensatory mutations, and long-range non-additive effects at the dimerization interface of the HIV capsid protein. *J. Mol. Biol.* 345:893–906
59. Kegel WK, van der Schoot P. 2006. Physical regulation of the self-assembly of tobacco mosaic virus coat protein. *Biophys. J.* 91:1501–12
60. Chandler D. 2005. Interfaces and the driving force of hydrophobic assembly. *Nature* 437:640–47
61. Hagan MF. 2010. Understanding the concentration dependence of viral capsid assembly kinetics: the origin of the lag time and identifying the critical nucleus size. *Biophys. J.* 98:1065–74
62. Zandi R, van der Schoot P, Reguera D, Kegel W, Reiss H. 2006. Classical nucleation theory of virus capsids. *Biophys. J.* 90:1939–48
63. Singh S, Zlotnick A. 2003. Observed hysteresis of virus capsid disassembly is implicit in kinetic models of assembly. *J. Biol. Chem.* 278:18249–55

64. Uetrecht C, Watts NR, Stahl SJ, Wingfield PT, Steven AC, Heck AJR. 2010. Subunit exchange rates in hepatitis B virus capsids are geometry- and temperature-dependent. *Phys. Chem. Chem. Phys.* 12:13368–71
65. Whitelam S, Rogers C, Pasqua A, Paavola C, Trent J, Geissler PL. 2009. The impact of conformational fluctuations on self-assembly: cooperative aggregation of archaeal chaperonin proteins. *Nano Lett.* 9:292–97
66. Sorger PK, Stockley PG, Harrison SC. 1986. Structure and assembly of turnip crinkle virus. II. Mechanism of reassembly in vitro. *J. Mol. Biol.* 191:639–58
67. Stray SJ, Bourne CR, Punna S, Lewis WG, Finn MG, Zlotnick A. 2005. A heteroaryldihydropyrimidine activates and can misdirect hepatitis B virus capsid assembly. *Proc. Natl. Acad. Sci. USA* 102:8138–43
68. Parent KN, Suhanovsky MM, Teschke CM. 2007. Polyhead formation in phage P22 pinpoints a region in coat protein required for conformational switching. *Mol. Microbiol.* 65:1300–10
69. Zlotnick A. 2003. Are weak protein-protein interactions the general rule in capsid assembly? *Virology* 315:269–74
70. Ruigrok RWH, Crepin T, Kolakofsky D. 2011. Nucleoproteins and nucleocapsids of negative-strand RNA viruses. *Curr. Opin. Microbiol.* 14:504–10
71. Speir JA, Munshi S, Wang GJ, Baker TS, Johnson JE. 1995. Structures of the native and swollen forms of cowpea chlorotic mottle virus determined by X-ray crystallography and cryoelectron microscopy. *Structure* 3:63–78
72. Hohn T. 1969. Role of RNA in the assembly process of bacteriophage fr. *J. Mol. Biol.* 43:191–200
73. Bancroft J, Hiebert E, Bracker CE. 1969. The effects of various polyanions on shell formation of some spherical viruses. *Virology* 39:924–30
74. Chen C, Kwak ES, Stein B, Kao CC, Dragnea B. 2005. Packaging of gold particles in viral capsids. *J. Nanosci. Nanotechnol.* 5:2029–33
75. Sun J, DuFort C, Daniel MC, Murali A, Chen C, et al. 2007. Core-controlled polymorphism in virus-like particles. *Proc. Natl. Acad. Sci. USA* 104:1354–59
76. Hu Y, Zandi R, Anavitarte A, Knobler CM, Gelbart WM. 2008. Packaging of a polymer by a viral capsid: the interplay between polymer length and capsid size. *Biophys. J.* 94:1428–36
77. Sikkema FD, Comellas-Aragones M, Fokkink RG, Verduin BJM, Cornelissen JJLM, Nolte RJM. 2007. Monodisperse polymer-virus hybrid nanoparticles. *Org. Biomol. Chem.* 5:54–57
78. Brasch M, Cornelissen JJLM. 2012. Relative size selection of a conjugated polyelectrolyte in virus-like protein structures. *Chem. Commun.* 48:1446–48
79. Kostiainen MA, Pietsch C, Hoogenboom R, Nolte RJM, Cornelissen JJLM. 2011. Temperature-switchable assembly of supramolecular virus-polymer complexes. *Adv. Funct. Mater.* 21:2012–19
80. Goicochea NL, De M, Rotello VM, Mukhopadhyay S, Dragnea B. 2007. Core-like particles of an enveloped animal virus can self-assemble efficiently on artificial templates. *Nano Lett.* 7:2281–90
81. Loo L, Guenther RH, Lommel SA, Franzen S. 2007. Encapsidation of nanoparticles by red clover necrotic mosaic virus. *J. Am. Chem. Soc.* 129:11111–17
82. Kwak M, Minten IJ, Anaya DM, Musser AJ, Brasch M, et al. 2010. Virus-like particles templated by DNA micelles: a general method for loading virus nanocarriers. *J. Am. Chem. Soc.* 132:7834–35
83. Chang CB, Knobler CM, Gelbart WM, Mason TG. 2008. Curvature dependence of viral protein structures on encapsidated nanoemulsion droplets. *ACS Nano* 2:281–86
84. Malyutin AG, Dragnea B. 2013. Budding pathway in the templated assembly of viruslike particles. *J. Phys. Chem. B* 117:10730–36
85. Cheng F, Tsvetkova IB, Khuong YL, Moore AW, Arnold RJ, et al. 2013. The packaging of different cargo into enveloped viral nanoparticles. *Mol. Pharm.* 10:51–58
86. Siber A, Bozic AL, Podgornik R. 2012. Energies and pressures in viruses: contribution of nonspecific electrostatic interactions. *Phys. Chem. Chem. Phys.* 14:3746–65
87. Zandi R, van der Schoot P. 2009. Size regulation of ss-RNA viruses. *Biophys. J.* 96:9–20
88. Hagan MF. 2009. A theory for viral capsid assembly around electrostatic cores. *J. Chem. Phys.* 130:114902
89. Zlotnick A, Porterfield JZ, Wang JCY. 2013. To build a virus on a nucleic acid substrate. *Biophys. J.* 104:1595–604
90. Belyi VA, Muthukumar M. 2006. Electrostatic origin of the genome packing in viruses. *Proc. Natl. Acad. Sci. USA* 103:17174–78

91. Hu T, Zhang R, Shklovskii BI. 2008. Electrostatic theory of viral self-assembly. *Physica A* 387:3059–64
92. Newman M, Chua PK, Tang FM, Su PY, Shih C. 2009. Testing an electrostatic interaction hypothesis of hepatitis B virus capsid stability by using an in vitro capsid disassembly/reassembly system. *J. Virol.* 83:10616–26
93. Venter PA, Marshall D, Schneemann A. 2009. Dual roles for an arginine-rich motif in specific genome recognition and localization of viral coat protein to RNA replication sites in flock house virus-infected cells. *J. Virol.* 83:2872–82
94. Le Pogam S, Chua PK, Newman M, Shih C. 2005. Exposure of RNA templates and encapsidation of spliced viral RNA are influenced by the arginine-rich domain of human hepatitis B virus core antigen (HBcAg 165–173). *J. Virol.* 79:1871–87
95. Ni P, Wang Z, Ma X, Das NC, Sokol P, et al. 2012. An examination of the electrostatic interactions between the N-terminal tail of the coat protein and RNA in brome mosaic virus. *J. Mol. Biol.* 419:284–300
96. Porterfield JZ, Dhason MS, Loeb DD, Nassal M, Stray SJ, Zlotnick A. 2010. Full-length hepatitis B virus core protein packages viral and heterologous RNA with similarly high levels of cooperativity. *J. Virol.* 84:7174–84
97. Kao CC, Ni P, Hema M, Huang XL, Dragnea B. 2011. The coat protein leads the way: an update on basic and applied studies with the brome mosaic virus coat protein. *Mol. Plant Pathol.* 12:403–12
98. Comas-Garcia M, Cadena-Nava RD, Rao ALN, Knobler CM, Gelbart WM. 2012. In vitro quantification of the relative packaging efficiencies of single-stranded RNA molecules by viral capsid protein. *J. Virol.* 86:12271–82
99. Perlmutter JD, Qiao C, Hagan MF. 2013. Viral genome structures are optimal for capsid assembly. *eLife* 2:e00632
100. van der Schoot P, Bruinsma R. 2005. Electrostatics and the assembly of an RNA virus. *Phys. Rev. E* 71:061928
101. Siber A, Podgornik R. 2008. Nonspecific interactions in spontaneous assembly of empty versus functional single-stranded RNA viruses. *Phys. Rev. E* 78:051915
102. Ting CL, Wu J, Wang ZG. 2011. Thermodynamic basis for the genome to capsid charge relationship in viral encapsidation. *Proc. Natl. Acad. Sci. USA* 108:16986–91
103. Manning GS. 1969. Limiting laws and counterion condensation in polyelectrolyte solutions I. Colligative properties. *J. Chem. Phys.* 51:924–33
104. Gopal A, Zhou Z, Knobler C, Gelbart W. 2012. Visualizing large RNA molecules in solution. *RNA* 18:284–99
105. Erdemci-Tandogan G, Wagner J, van der Schoot P, Podgornik R, Zandi R. 2014. RNA topology remolds electrostatic stabilization of viruses. *Phys. Rev. E* 89:032707
106. Yoffe AM, Prinsen P, Gopal A, Knobler CM, Gelbart WM, Ben-Shaul A. 2008. Predicting the sizes of large RNA molecules. *Proc. Natl. Acad. Sci. USA* 105:16153–58
107. Stehle T, Gamblin SJ, Yan YW, Harrison SC. 1996. The structure of simian virus 40 refined at 3.1 Å resolution. *Structure* 4:165–82
108. Cadena-Nava RD, Comas-Garcia M, Garmann RF, Rao ALN, Knobler CM, Gelbart WM. 2012. Self-assembly of viral capsid protein and RNA molecules of different sizes: requirement for a specific high protein/RNA mass ratio. *J. Virol.* 86:3318–26
109. Garmann RF, Comas-Garcia M, Gopal A, Knobler CM, Gelbart WM. 2014. The assembly pathway of an icosahedral single-stranded RNA virus depends on the strength of inter-subunit attractions. *J. Mol. Biol.* 426:1050–60
110. Perlmutter JD, Perkett MR, Hagan MF. 2014. Pathways for virus assembly around nucleic acids. *J. Mol. Biol.* 426:3148–65
111. Zhang R, Linse P. 2013. Icosahedral capsid formation by capsomers and short polyions. *J. Chem. Phys.* 138:154901
112. Zhang R, Wernersson E, Linse P. 2013. Icosahedral capsid formation by capsomer subunits and a semiflexible polyion. *RSC Adv.* 3:25258–67
113. Comas-Garcia M, Garmann RF, Singaram SW, Ben-Shaul A, Knobler CM, Gelbart WM. 2014. Characterization of viral capsid protein self-assembly around short single-stranded RNA. *J. Phys. Chem. B* 118:7510–19

114. Kivenson A, Hagan M. 2010. Mechanisms of viral capsid assembly around a polymer. *Biophys. J.* 99:619–28
115. Hu T, Shklovskii BI. 2007. Kinetics of viral self-assembly: role of the single-stranded RNA antenna. *Phys. Rev. E* 75:051901
116. McPherson A. 2005. Micelle formation and crystallization as paradigms for virus assembly. *Bioessays* 27:447–58
117. Hagan MF. 2008. Controlling viral capsid assembly with templating. *Phys. Rev. E* 77:051904
118. Devkota B, Petrov AS, Lemieux S, Boz MB, Tang L, et al. 2009. Structural and electrostatic characterization of pariacoto virus: implications for viral assembly. *Biopolymers* 91:530–38
119. Garmann RF, Comas-Garcia M, Koay MS, Cornelissen JJLM, Knobler CM, Gelbart WM. 2014. The role of electrostatics in the assembly pathway of a single-stranded RNA virus. *J. Virol.* 88:10472–79
120. Routh A, Domitrovic T, Johnson JE. 2012. Host RNAs, including transposons, are encapsidated by a eukaryotic single-stranded RNA virus. *Proc. Natl. Acad. Sci. USA* 109:1907–12
121. Larson SB, Koszelak S, Day J, Greenwood A, Dodds JA, McPherson A. 1993. Double-helical RNA in satellite tobacco mosaic virus. *Nature* 361:179–82
122. Larson SB, Day J, Greenwood A, McPherson A. 1998. Refined structure of satellite tobacco mosaic virus at 1.8 Å resolution. *J. Mol. Biol.* 277:37–59
123. Larson SB, McPherson A. 2001. Satellite tobacco mosaic virus RNA: structure and implications for assembly. *Curr. Opin. Struct. Biol.* 11:59–65
124. Schroeder SJ, Stone JW, Bleckley S, Gibbons T, Mathews DM. 2011. Ensemble of secondary structures for encapsidated satellite tobacco mosaic virus RNA consistent with chemical probing and crystallography constraints. *Biophys. J.* 101:167–75
125. Zeng Y, Larson S, Heitsch C, McPherson A, Harvey S. 2012. A model for the structure of satellite tobacco mosaic virus. *J. Struct. Biol.* 180:110–16
126. Archer EJ, Simpson MA, Watts NJ, O'Kane R, Wang B, et al. 2013. Long-range architecture in a viral RNA genome. *Biochemistry* 52:3182–90
127. Athavale SS, Gossett JJ, Bowman JC, Hud NV, Williams LD, Harvey SC. 2013. In vitro secondary structure of the genomic RNA of satellite tobacco mosaic virus. *PLoS ONE* 8:e54384
128. Rao A. 2006. Genome packaging by spherical plant RNA viruses. *Annu. Rev. Phytopathol.* 44:61–87
129. Stockley PG, Twarock R, Bakker SE, Barker AM, Borodavka A, et al. 2013. Packaging signals in single-stranded RNA viruses: nature's alternative to a purely electrostatic assembly mechanism. *J. Biol. Phys.* 39:277–87
130. Pappalardo L, Kerwood DJ, Pelczer I, Borer PN. 1998. Three-dimensional folding of an RNA hairpin required for packaging HIV-1. *J. Mol. Biol.* 282:801–18
131. Lu K, Heng X, Summers MF. 2011. Structural determinants and mechanism of HIV-1 genome packaging. *J. Mol. Biol.* 410:609–33
132. D'Souza V, Summers MF. 2005. How retroviruses select their genomes. *Nat. Rev. Microbiol.* 3:643–55
133. Bunka DHJ, Lane SW, Lane CL, Dykeman EC, Ford RJ, et al. 2011. Degenerate RNA packaging signals in the genome of satellite tobacco necrosis virus: implications for the assembly of a $T = 1$ capsid. *J. Mol. Biol.* 413:51–65
134. Dykeman EC, Grayson NE, Toropova K, Ranson NA, Stockley PG, Twarock R. 2011. Simple rules for efficient assembly predict the layout of a packaged viral RNA. *J. Mol. Biol.* 408:399–407
135. Dykeman EC, Stockley PG, Twarock R. 2013. Packaging signals in two single-stranded RNA viruses imply a conserved assembly mechanism and geometry of the packaged genome. *J. Mol. Biol.* 425:3235–49
136. ElSawy KM, Caves LSD, Twarock R. 2010. The impact of viral RNA on the association rates of capsid protein assembly: bacteriophage MS2 as a case study. *J. Mol. Biol.* 400:935–47
137. Morton VL, Dykeman EC, Stonehouse NJ, Ashcroft AE, Twarock R, Stockley PG. 2010. The impact of viral RNA on assembly pathway selection. *J. Mol. Biol.* 401:298–308
138. Dykeman EC, Stockley PG, Twarock R. 2014. Solving a Levinthal's paradox for virus assembly identifies a unique antiviral strategy. *Proc. Natl. Acad. Sci. USA* 111:5361–66
139. Johnson JM, Willits DA, Young MJ, Zlotnick A. 2004. Interaction with capsid protein alters RNA structure and the pathway for in vitro assembly of cowpea chlorotic mottle virus. *J. Mol. Biol.* 335:455–64

140. Annamalai P, Rofail F, DeMason DA, Rao ALN. 2008. Replication-coupled packaging mechanism in positive-strand RNA viruses: synchronized coexpression of functional multigenome RNA components of an animal and a plant virus in *Nicotiana benthamiana* cells by agroinfiltration. *J. Virol.* 82:1484–95
141. Hurley JH, Boura E, Carlson LA, Róycki B. 2010. Membrane budding. *Cell* 143:875–87
142. Sundquist WI, Krausslich HG. 2012. HIV-1 assembly, budding, and maturation. *Cold Spring Harb. Perspect. Med.* 2:a006924
143. Welsch S, Müller B, Kräusslich HG. 2007. More than one door: budding of enveloped viruses through cellular membranes. *FEBS Lett.* 581:2089–97
144. Garoff H, Sjöberg M, Cheng RH. 2004. Budding of alphaviruses. *Virus Res.* 106:103–16
145. McMahon HT, Gallop JL. 2005. Membrane curvature and mechanisms of dynamic cell membrane remodelling. *Nature* 438:590–96
146. Doherty GJ, McMahon HT. 2009. Mechanisms of endocytosis. *Annu. Rev. Biochem.* 78:857–902
147. Taylor MP, Koyuncu OO, Enquist LW. 2011. Subversion of the actin cytoskeleton during viral infection. *Nat. Rev. Microbiol.* 9:427–39
148. Gladnikoff M, Shimoni E, Gov NS, Rousso I. 2009. Retroviral assembly and budding occur through an actin-driven mechanism. *Biophys. J.* 97:2419–28
149. Balasubramaniam M, Freed EO. 2011. New insights into HIV assembly and trafficking. *Physiology* 26:236–51
150. Rossman JS, Lamb RA. 2013. Viral membrane scission. *Annu. Rev. Cell Dev. Biol.* 29:551–69
151. Matthews R, Likos C. 2012. Influence of fluctuating membranes on self-assembly of patchy colloids. *Phys. Rev. Lett.* 109:178302
152. Matthews R, Likos CN. 2013. Dynamics of self-assembly of model viral capsids in the presence of a fluctuating membrane. *J. Phys. Chem. B* 117:8283–92
153. Ruiz-Herrero T, Hagan MF. 2014. Virus assembly on a membrane is facilitated by membrane microdomains. *Biophys. J.* In press. doi: 10.1016/j.bpj.2014.12.017
154. Helfrich W. 1973. Elastic properties of lipid bilayers: theory and possible experiments. *Z. Nat. C* 28:693–703
155. Tzlil S, Deserno M, Gelbart WM, Ben-Shaul A. 2004. A statistical-thermodynamic model of viral budding. *Biophys. J.* 86:2037–48
156. Lerner DM, Deutsch JM, Oster GF. 1993. How does a virus bud? *Biophys. J.* 65:73–79
157. Barrow E, Nicola AV, Liu J. 2013. Multiscale perspectives of virus entry via endocytosis. *Virol. J.* 10:177
158. Zhang R, Nguyen T. 2008. Model of human immunodeficiency virus budding and self-assembly: role of the cell membrane. *Phys. Rev. E* 78:051903
159. Waheed AA, Freed EO. 2010. The role of lipids in retrovirus replication. *Viruses* 2:1146–80
160. Rossman JS, Lamb RA. 2011. Influenza virus assembly and budding. *Virology* 411:229–36
161. Prevelige PE Jr. 2011. New approaches for antiviral targeting of HIV assembly. *J. Mol. Biol.* 410:634–40
162. Zlotnick A, Mukhopadhyay S. 2011. Virus assembly, allostery and antivirals. *Trends Microbiol.* 19:14–23
163. Plevka P, Perera R, Yap ML, Cardosa J, Kuhn RJ, Rossmann MG. 2013. Structure of human enterovirus 71 in complex with a capsid-binding inhibitor. *Proc. Natl. Acad. Sci. USA* 110:5463–67
164. Colibus LD, Wang X, Spyrou JAB, Kelly J, Ren J, et al. 2014. More-powerful virus inhibitors from structure-based analysis of HEV71 capsid-binding molecules. *Nat. Struct. Mol. Biol.* 21:282–88
165. Katen SP, Chirapu SR, Finn MG, Zlotnick A. 2010. Trapping of hepatitis B virus capsid assembly intermediates by phenylpropenamide assembly accelerators. *ACS Chem. Biol.* 5:1125–36
166. Katen SP, Tan Z, Chirapu SR, Finn MG, Zlotnick A. 2013. Assembly-directed antivirals differentially bind quasiequivalent pockets to modify hepatitis B virus capsid tertiary and quaternary structure. *Structure* 21:1406–16
167. Bamunusinghe D, Seo JK, Rao ALN. 2011. Subcellular localization and rearrangement of endoplasmic reticulum by brome mosaic virus capsid protein. *J. Virol.* 85:2953–63